International Journal of Microscale and Nanoscale … ISSN: 1949-4955
Volume 5, Number 2

MIXED CONVECTION FLOW IN A VERTICAL CHANNEL FILLED WITH A FLUID-SATURATED POROUS MEDIUM DIVIDED BY A PERFECTLY CONDUCTIVE BAFFLE

J. C. Umavathi[1], I. C. Liu[2] and Ali J. Chamkha[3*]
[1]Department of Mathematics, Gulbarga University, Karnataka, India
[2]Department of Civil Engineering, National Chi Nan University,
Nantou, Taiwan, R.O.C
[3]Manufacturing Engineering Department,
The Public Authority for Applied Education and Training,
Shuweikh, Kuwait

ABSTRACT

This study aims to investigate fully-developed laminar mixed convection flow in a vertical channel with a thin and perfectly conductive baffle, containing a viscous fluid-saturated porous medium. Uniform wall temperatures with asymmetric heating, taking into account the viscous and Darcy dissipations in energy equation, have been considered. The nonlinear governing equations are solved analytically by the perturbation method and numerically by the finite-difference method. The influence of the porous parameter, ratio of Grashof number to Reynolds number, Brinkman number, viscosity ratio and baffle position on the velocity, temperature distribution and the Nusselt number variation for the system is explored. It is found that the velocity and temperature profiles are distorted by the effect of porous parameter, Brinkman number, Grashof number to Reynolds number and the viscosity ratio. The increase in the porous parameter and Brinkman number results in the enhancement in temperature, while the temperature decreases with the increase of the viscosity ratio. Flow reversal can be also found even in the double-passage channel with suitable combination of parameters. Heat transfer rates at both walls are enhanced by increasing values of the porous parameter.

Keywords: double-passage channel, baffle, Darcy-Brinkman equation, viscous and Darcy dissipations, heat transfer.

* Corresponding author: E-mail address: achamkha@yahoo.com (A.J. Chamkha).

NOMENCLATURE

b	channel width $[\mathrm{m}]$
b^*	width of passage 1 $[\mathrm{m}]$
Br	Brinkman number
C_p	specific heat at constant pressure $[\mathrm{J\,kg^{-1}\,K^{-1}}]$
g	gravitational acceleration $[\mathrm{ms^{-1}}]$
Gr	Grashof number
k_{eff}	effective thermal conductivity $[\mathrm{W\,m^{-1}K^{-1}}]$
m	viscosity ratio
p	pressure $[\mathrm{Nm^{-2}}]$
p^*	dimensionless pressure
Re	Reynolds number
s	permeability of the porous media $[\mathrm{m^2}]$
T	temperature $[\mathrm{K}]$
u	axial velocity $[\mathrm{m\,s^{-1}}]$
U	dimensionless velocity
x	axial coordinate $[\mathrm{m}]$
X	dimensionless axial coordinate
y	transverse coordinate $[\mathrm{m}]$
Y	dimensionless transverse coordinate

Greek symbols

β	volumetric coefficient of thermal expansion $[\mathrm{K^{-1}}]$
γ	pressure gradient parameter
θ	dimensionless temperature
μ	dynamic viscosity $[\mathrm{Pa\,s}]$
μ_{eff}	effective viscosity in porous medium $[\mathrm{Pa\,s}]$
υ	kinematic viscosity $[\mathrm{m^2s^{-1}}]$
ρ	density $[\mathrm{kg\,m^{-3}}]$
σ	porous parameter

Subscripts

b	bulk
c	cold wall
h	hot wall
r	reference
1	value in stream 1
2	value in stream 2

1. INTRODUCTION

The methods to effectively enhance heat transfer are of interest for many researchers now. Among the heat transfer enhancement schemes, those related to the mixed convection within a vertical channel receive much attention because they often occur in practice, such as in electronic cooling equipments, cooling passages of turbine blades and heat exchangers, etc. The well-known concepts of passive techniques of convective heat transfer enhancement [1-3] are to increase the heat transfer area and/or the convective heat transfer coefficient in terms of (a) mixing the main flow and/or the flow in the wall region as by using rough surface, inserts, etc.; (b) reducing the flow boundary layer thickness by using offset strip fins, jet impingement, etc.; (c) creating the rotating and/or the secondary flow by using swirl flow device, duct rotation, etc.; (d) raising the turbulence intensity by using rough surface, turbulence promoter, etc.

The most commonly used technique for internal cooling enhancement is the placement of periodic ribs. Ribs are generally mounted on the heat transfer surface, which disturb the boundary layer growth and enhance the heat transfer between the surface and the fluid. In addition to ribs and impingement, a third common internal cooling enhancement technique is the placement of internal flow swirls, tape twisters, or baffles. The convective heat transfer in a vertical channel could be enhanced by using special inserts which can be specially designed to increase the included angle between the velocity vector and the temperature gradient vector rather than to promote turbulence. This increases the rate of heat transfer without a considerable drop in the pressure (Guo et al. [4]). A plane baffle may be used as an insert to enhance the rate of heat transfer in the channel. A thin and perfectly conductive baffle is used so as to avoid a considerable increase in the transverse thermal resistance into the channel. Although viscous dissipation is usually neglected in low-speed and low-viscosity flows through conventionally-sized channels of short lengths, for flows through relatively long pipelines, viscous dissipation may become important (Tso and Mahulikar [5]). Cheng et al. [6] studied analytically heat transfer aspects of a laminar fully developed forced-convection within an asymmetrically heated horizontal double-passage channel and concluded that the thermal characteristics of the fully developed flow could be significantly affected by the position of the baffle, the pressure gradient ratio and the thermal boundary conditions. Similar mixed convection problem in a vertical double-passage channel has been investigated analytically by Salah El-Din [7]. His results showed that the presence of the baffle may lead to a higher value of Nusselt number according to the baffle position and the value of Gr/Re

Dutta and Dutta [8] reported experimental results of the enhancement of heat transfer with inclined solid and perforated baffles. In that study, the effects of baffle size, position, and orientation were studied for internal cooling heat transfer augmentation. Chen and Chen [9] experimental results showed that for small baffle widths, the local heat transfer coefficient decreases with an increase in the baffle-wall gap. For large baffle widths, there is an optimum distance between the baffle and the solid wall which gives rise to a higher heat transfer coefficient. Shiina et al. [10] experimentally investigated the shell side heat transfer and pressure drop in counter flowing water on the basis of the overall heat transfer coefficient. They found that low-pressure drop spacer improved the heat transfer performance about 1.2 times more than the standard spacer, regardless of the pumping power. More recently Chang and Shiau [11] studied numerically the effects of a horizontal baffle on the heat transfer characteristics of pulsating opposing mixed convection in a parallel vertical open channel. They found that the flow pulsation with a baffle gives the optimal heat transfer. Also with large Reynolds number, the inlet flow pulsation dominates the velocity field in the channel. Dutta and Hossain [12] experimentally investigated the local heat transfer characteristics and the associated frictional head loss in a rectangular channel with inclined solid and perforated baffles. One main result they found is that the inner placement of baffles augments the overall heat transfer significantly by combining both jet impingement and the boundary layer separation. The strong dependence of local Nusselt number distribution by the baffle position, orientation and geometry of the second baffle plate is another one important conclusion.

For flows through channels with baffles, the length-to-width ratio becomes large as the position of the inserted baffle is adjusted near the wall, therefore the effect of viscous dissipation, under this situation, should be considered. Salah El-Din [13] investigated numerically mixed convection in a vertical double-passage channel, taking into account the effect of viscous dissipation. He drew the conclusion that the increase in Brinkman number decreases the Nusselt number on the hot wall and increases that on the cold wall especially when the baffle becomes near the hot wall or the cold wall, respectively.

The above literature review indicates that most of the articles concern about convection in vertical channels with inserts for clear viscous fluids. Many industrial processes relied on the utilization of porous media as an effective mean for transporting and storing energy. Due to the large surface-to-volume ratio, the thermal response of these units is relatively fast as compared to other developed energy carrier devices. Common examples of industrial applications include management of geothermal systems, heat pipes, phase change applications and transpiration cooling. Such applications are cited in Tien and Vafai [14] and Amiri and Vafai [15]. Recently Weidman and Medina [16] studied natural convection in a vertical slot filled with a fluid-saturated porous medium modeled by the Brinkman equation, giving the relative importance of porous media from open to capped ends. Keeping in view the enormous applications of porous media, motivated the authors to study the present problem. The objective of this work is to explore the characteristics of flow behavior and heat transfer of fluid-saturated porous medium contained in a vertical channel with a perfectly conductive baffle, including the effects of viscous and Darcy dissipations.

2. PROBLEM FORMULATION

Consider a steady, laminar fully-developed mixed convective flow in an open-ended vertical parallel plane channel filled with a porous material. The channel is divided into two passages by means of a perfectly conductive thin baffle, for which the transverse thermal resistance can be neglected (Cheng et al. [6] and Salah El Din [7, 13]). The fluid is assumed to be Newtonian and the porous medium is isotropic and homogeneous. The conservation equations for the porous region are based on a non-Darcian model, incorporating the Brinkman extension in the momentum equation, viscous dissipation and Darcy dissipation terms in the energy equation (Nield and Bejan [17]). The fluid enters the channel with a uniform upward vertical velocity and constant temperature. The channel walls are subjected to different constant temperatures. It is assumed that all physical properties, except for the density, are constant. The Oberbeck-Boussinesq approximation is supposed to hold (Rajagopal [18]). The $\underline{x}$-axis is chosen parallel to the gravitational field, but with opposite direction and y-axis is transverse to the channel walls as shown in Figure 1.

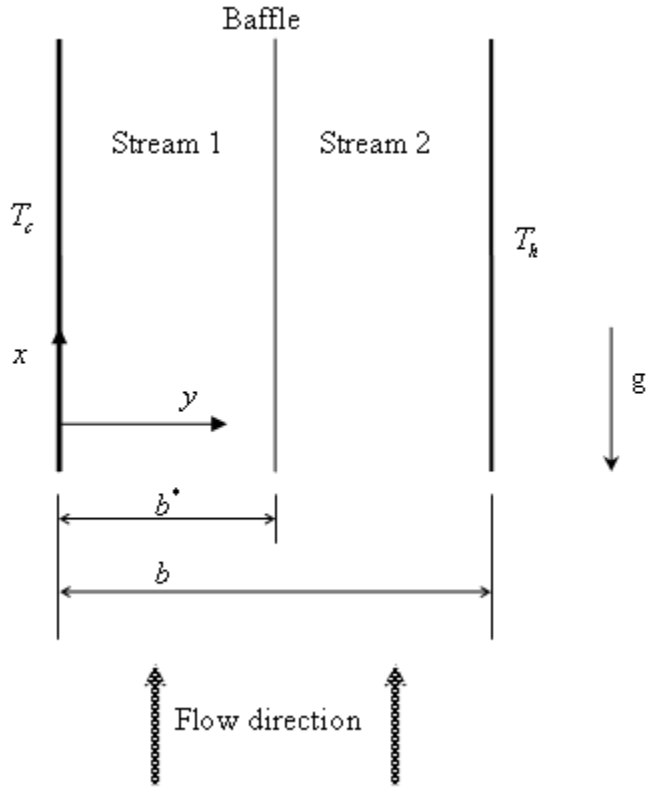

Figure 1. Physical configuration of the double-passage channel.

For a fully-developed flow, it is assumed that the transverse velocity and temperature gradients in the axial direction are zero. With the assumptions made above, the governing equations of motion and energy reduce to (Nield and Bejan [17] and Barletta [19]),

$$\frac{\mu_{eff}}{\rho_r}\frac{d^2u_i}{dy^2} = -g\beta\left(T_i - T_r\right) + \frac{1}{\rho_r}\frac{dp_i}{dx} + \frac{\mu u_i}{\rho_r s} \tag{1}$$

$$k_{eff}\frac{d^2T_i}{dy^2} + \mu_{eff}\left(\frac{du_i}{dy}\right)^2 + \frac{\mu {u_i}^2}{s} = 0 \tag{2}$$

The subscript i denotes either Stream 1 or Stream 2. We note that the second and third terms in Eq. (2) are viscous and Darcy dissipations, respectively. Viscous dissipation accounts for heat loss by frictional forces of the fluid phase and Darcy dissipation for heat loss by frictional forces of solid phase. Gilver and Altobelli [20] experimentally showed that fluid viscosity and the Brinkman viscosity (i.e., effective viscosity) are not the same. Thus, the ratio of the fluid viscosity and Brinkman viscosity is taken as m^2.

The boundary conditions are

$$y = 0: \qquad u_1 = 0, \qquad T_1 = T_c \tag{3a}$$

$$y = b^*: \qquad u_1 = u_2 = 0, \quad T_1 = T_2, \quad \frac{dT_1}{dy} = \frac{dT_2}{dy} \tag{3b}$$

$$y = b: \qquad u_2 = 0, \qquad T_2 = T_h \tag{3c}$$

The average of the walls temperature is chosen as the reference temperature (see Barletta and Zanchini [21]), i.e.

$$T_r = \frac{T_c + T_h}{2} \tag{4}$$

Equations (1)-(3) can be written in a dimensionless form by employing the dimensionless quantities

$$X = \frac{x}{b\,\mathrm{Re}},\ Y = \frac{y}{b},\ Y^* = \frac{b^*}{b},\ U = \frac{u}{u_r},\ \theta = \frac{T - T_r}{T_h - T_c},\ p^* = \frac{p}{\rho_r {u_r}^2},\ \mathrm{Re} = \frac{u_r b}{\upsilon},$$
$$Gr = \frac{g\beta\left(T_h - T_c\right)b^3}{\upsilon^2},\quad Br = \frac{\mu {u_r}^2}{k_{eff}\left(T_h - T_c\right)},\ m^2 = \frac{\mu}{\mu_{eff}},\ \sigma^2 = \frac{b^2}{s},\ \gamma = \frac{dp^*}{dX} \tag{5}$$

The reference velocity u_r is defined by

$$u_r = \frac{1}{b}\int_0^b u\,dy \tag{6}$$

Using (5), Eqs. (1)-(3) become

$$\frac{d^2U_i}{dY^2} = -\frac{Gr}{\mathrm{Re}} m^2\theta_i + m^2\gamma_i + m^2\sigma^2 U_i \tag{7}$$

$$\frac{d^2\theta_i}{dY^2} + \frac{Br}{m^2}\left(\frac{dU_i}{dY}\right)^2 + Br\sigma^2 U_i^{\,2} = 0 \tag{8}$$

subject to the boundary conditions

$$Y = 0; \quad U_1 = 0, \quad \theta_1 = -\frac{1}{2} \tag{9a}$$

$$Y = Y^*; \quad U_1 = U_2 = 0, \quad \theta_1 = \theta_2\ , \quad \frac{d\theta_1}{dy} = \frac{d\theta_2}{dy} \tag{9b}$$

$$Y = 1; \quad U_2 = 0, \quad \theta_2 = \frac{1}{2} \tag{9c}$$

The pressure gradient γ in Eq. (7) is assumed to be constant.

Since the pressure gradients in both passages can be controlled at one's disposal, the respective flowrate is assumed to be distributed proportional to the area of each passage. Therefore, the conservation of mass considered at any cross section of the passage gives

$$\int_0^{Y^*} U_1\, dY = Y^* \tag{10}$$

and

$$\int_{Y^*}^{1} U_2\, dY = 1 - Y^* \tag{11}$$

The Nusselt numbers, which are physically relevant, at the cold and hot walls are defined

$$Nu_c = \frac{b}{T_h - T_c}\left(\frac{dT_1}{dy}\right)_{y=0} = \left(\frac{d\theta_1}{dY}\right)_{Y=0} \tag{12a}$$

$$Nu_h = \frac{b}{T_h - T_c}\left(\frac{dT_2}{dy}\right)_{y=b} = \left(\frac{d\theta_2}{dY}\right)_{Y=1} \tag{12b}$$

3. ANALYTICAL SOLUTION

Equations (7) and (8) are coupled nonlinear ordinary differential equations and hence, finding exact solutions is out of scope. However, for smaller values of the Brinkman number approximate solutions can be extracted through the perturbation method. The Brinkman number is usually small and hence, regular perturbation method can be strongly justified. Adopting this technique, solutions for the velocity and temperature are assumed in the form

$$U_i = \left(U_{i0},\ \theta_{i0}\right) + \varepsilon\left(U_{i1}, \theta_{i1}\right) + \cdots \tag{13}$$

where ε represents the small Brinkman parameter Br and the first order terms give a correction to U_{i0} and θ_{i0}, accounting for dissipative effects. Substituting Eq. (13) into Eqs. (7) and (8) and equating the coefficients of the like powers of ε, we get

Zeroth-order equations:

$$\frac{d^2U_{i0}}{dY^2} + \frac{Gr}{\mathrm{Re}} m^2\theta_{i0} - m^2\gamma_i - m^2\sigma^2 U_{i0} = 0 \tag{14}$$

$$\frac{d^2\theta_{i0}}{dY^2} = 0 \tag{15}$$

First-order equations:

$$\frac{d^2U_{i1}}{dY^2} + \frac{Gr}{\mathrm{Re}} m^2\theta_{i1} - m^2\sigma^2 U_{i1} = 0 \tag{16}$$

$$\frac{d^2\theta_{i1}}{dy^2} + \frac{1}{m^2}\left(\frac{dU_{i0}}{dY}\right)^2 + \sigma^2 U_{i1}^2 = 0 \tag{17}$$

Invoking Eq. (13) into Eq. (9), the boundary conditions may be written as

Zeroth-order boundary conditions

$$U_{10} = 0; \quad \text{at} \quad Y = 0 : \theta_{10} = -1/2 \quad \text{at} \quad Y = 0 \tag{18a}$$

$$U_{20} = 0; \quad \text{at} \quad Y = 1 : \theta_{20} = 1/2 \quad \text{at} \quad Y = 1 \tag{18b}$$

$$U_{10} = 0; \quad \text{at} \quad Y = Y^* :\ \theta_{10} = \theta_{20} \quad \text{at} \quad Y = Y^* \tag{18c}$$

$$U_{20} = 0; \quad \text{at} \quad Y = Y^* : \frac{d\theta_{10}}{dY} = \frac{d\theta_{20}}{dY} \quad \text{at} \quad Y = Y^* \tag{18d}$$

First-order boundary conditions

$$U_{11} = 0 \quad \text{at} \quad Y = 0 : \theta_{11} = 0 \quad \text{at} \quad Y = 0 \tag{19a}$$

$$U_{21} = 0 \quad \text{at} \quad Y = 1 : \theta_{21} = 0 \quad \text{at} \quad Y = 1 \tag{19b}$$

$$U_{11} = 0 \quad \text{at} \quad Y = Y^* :\ \theta_{11} = \theta_{21} \quad \text{at} \quad Y = Y^* \tag{19c}$$

$$U_{21} = 0 \quad \text{at} \quad Y = Y^* :\ \frac{d\theta_{11}}{dY} = \frac{d\theta_{21}}{dY} \quad \text{at} \quad Y = Y^* \tag{19d}$$

Solving the zeroth-order equations (14) and (15) subject to boundary conditions (18a)-(18d), we obtain

Stream 1

$$\theta_{10} = Y - 0.5 \tag{20}$$

$$U_{10} = d_1 \cosh(\alpha Y) + d_2 \sinh(\alpha Y) + l_1 Y + l_2 \tag{21}$$

Stream 2

$$\theta_{20} = Y - 0.5 \tag{22}$$

$$U_{20} = d_3 \cosh(\alpha Y) + d_4 \sinh(\alpha Y) + l_1 Y + l_3 \tag{23}$$

Similarly, the solutions for the first-order equations (16) and (17) using the boundary conditions (19a)-(19d) are given by

Stream 1

$$\theta_{11} = f_1 \cosh(2\alpha Y) + f_2 \sinh(2\alpha Y) + f_3 Y \cosh(\alpha Y) + f_4 Y \sinh(\alpha Y) + f_5 \cosh(\alpha Y) + f_6 \sinh(\alpha Y) + f_7 Y^4 + f_8 Y^3 + f_9 Y^2 + c_1 Y + c_2 \tag{24}$$

$$U_{11} = d_5 \cosh(\alpha Y) + d_6 \sinh(\alpha Y) + f_{10} \cosh(2\alpha Y) + f_{11} \sinh(2\alpha Y) + f_{12} Y^2 \cosh(\alpha Y) + f_{13} Y^2 \sinh(\alpha Y) + f_{14} Y \cosh(\alpha Y) + f_{15} Y \sinh(\alpha Y) + f_{16} Y^4 + f_{17} Y^3 + f_{18} Y^2 + f_{19} Y + f_{20} \tag{25}$$

Stream 2

$$\theta_{21} = f_{21} \cosh(2\alpha Y) + f_{22} \sinh(2\alpha Y) + f_{23} Y \cosh(\alpha Y) + f_{24} Y \sinh(\alpha Y) + f_{25} \cosh(\alpha Y) + f_{26} \sinh(\alpha Y) + f_{27} Y^4 + f_{28} Y^3 + f_{29} Y^2 + c_3 Y + c_4 \tag{26}$$

$$U_{21} = d_7 \cosh(\alpha Y) + d_8 \sinh(\alpha Y) + f_{30} \cosh(2\alpha Y) + f_{31} \sinh(2\alpha Y) + f_{32} Y^2 \cosh(\alpha Y) + f_{33} Y^2 \sinh(\alpha Y) + f_{34} Y \cosh(\alpha Y) + f_{35} Y \sinh(\alpha Y) + f_{36} Y^4 + f_{37} Y^3 + f_{38} Y^2 + f_{39} Y + f_{40} \tag{27}$$

The constants appeared in above Eqs. (24) to (27) are omitted for simplicity.

4. NUMERICAL SOLUTION

Since Eqs. (7) and (8) do not pose closed-form solutions for all values of non-zero Brinkman number and thus the perturbation method does not give complete solution, a numerical solution is sought. Due to the complexity of the problem, the effects of γ_1 and γ_2 are considered only for zeroth order solutions. For analytical solutions, Eqs. (10) and (11) are approximated as

$$\int_0^{Y^*} U_{10}\, dY = Y^* \tag{28}$$

and

$$\int_{Y^*}^{1} U_{20}\, dY = 1 - Y^* \tag{29}$$

The use of Eqs. (28) and (29) is relaxed to Eqs. (10) and (11) in numerical solutions. Since an iterated scheme is appropriate for solving the present problem, the finite-difference method is employed. The procedure of solving this problem is outlined as follows:

(i) Assign values to the position of the baffle Y^*, mixed convection parameter Gr/Re, porous parameter σ and the viscosity ratio m.

(ii) Guess the pressure gradients γ_1 and γ_2, and solve the velocity and temperature fields from Eqs. (7), (8) subject to boundary condition (9) using a finite-difference scheme of second-order accuracy.

(iii) When all values of the solutions between two successive iterations in the computational domain are less than a small value, say 10^{-14}, a trial solution is found.

(iv) The trial solution, in general, does not satisfy the constraints Eqs. (10) and (11), hence, a Newton-Raphson scheme is used, in step (ii), to find the corrected values of pressure gradients within suitable tolerance 10^{-6}. At this moment, the solutions to the present problem are supposed to be sought.

In each passage, a uniform grid system with 100 grids is employed, therefore, a smaller size in the narrower passage will be used. In addition, the double precision accuracy of numerics in FORTRAN is chosen. It is noted that the pressure gradients obtained from Eqs. (28) and (29) can be used as the initial guesses in step (ii) for quick convergence. To verify the numerical code, the simplified cases are compared. For pure viscous fluids in both passages the analytical solutions for temperature obtained in Eqs. (20) and (22) admit $Nu_c = Nu_h = 1$. The numerical solutions are

$$Y^* = 0.2,\ \ Nu_c = 1.00000000,\ \ Nu_h = 0.99999999,$$
$$Y^* = 0.5,\ \ Nu_c = 0.99999999,\ \ Nu_h = 1.00000000,$$
$$Y^* = 0.8,\ \ Nu_c = 1.00000000,\ \ Nu_h = 0.99999999.$$

When there is no buoyancy forces ($Gr/\mathrm{Re} = 0$) and pure viscous fluids are considered, the analytical solutions for momentum equations give $\gamma_1 = -12/Y^{*2}$ and $\gamma_2 = -12/(1-Y^*)^2$. The numerical code finds the values

$$Y^* = 0.2,\ \ \gamma_1 = -300.9999910,\ \ \gamma_2 = -18.7500001,$$
$$Y^* = 0.5,\ \ \gamma_1 = \gamma_2 = -48.000000,$$
$$Y^* = 0.8,\ \ \gamma_1 = -18.7499994,\ \ \gamma_2 = -300.0000358.$$

Thus, the accuracy of the numerical code can be confirmed.

5. RESULTS AND DISCUSSION

The objective of the present study is to examine the characteristics of mixed convection of a permeable fluid in a vertical channel containing a thin conducting baffle, considering the effect of viscous and Darcy dissipations. First of all, the analytical and numerical results are compared in Figure 2 for the velocity and temperature fields when the baffle is placed in the mid-section of the channel.

In these figures, the Brinkman numbers are taken to be 0, 0.05 and 0.1 for the respective curves. For zero Brinkman number, the analytical and numerical solutions coincide. It can be observed that for small value of Br, both the velocity and temperature profiles for the analytical and numerical results differ a little, whereas for large values of Br, the derivation between the numerical and analytical results for the velocity field differ much than that for the temperature field. This reflects the fact that the pressure gradients for velocity are determined analytically only by Eqs. (28) and (29) rather than those employed by numerical procedure using Eqs. (10) and (11). However, the zero-order solution can be used as an initial guess for numerical computation. The following graphs are drawn using the finite-difference numerical solutions only.

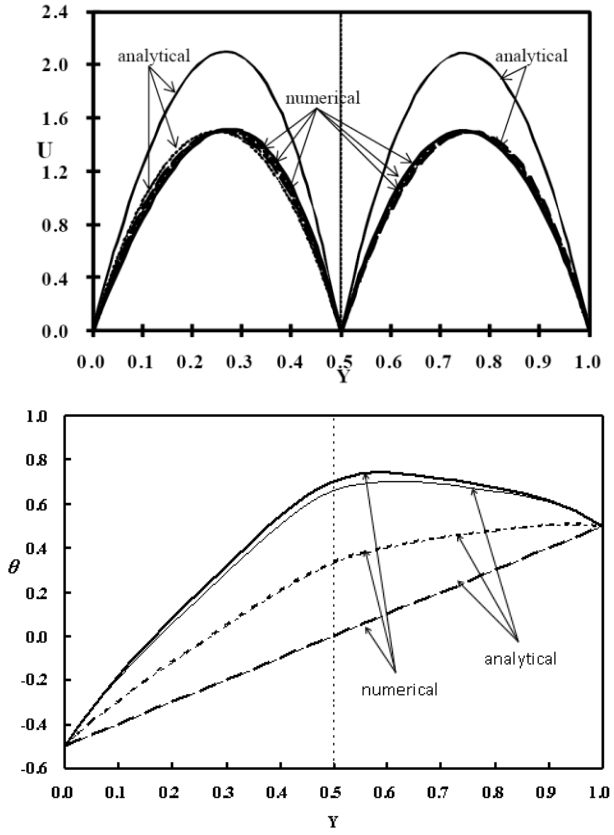

Figure 2. Comparison of analytical and numerical solutions with $Gr/\mathrm{Re}=50$, $\sigma=2.$, $m=1$; dashed $Br=0$, dotted $Br=0.05$, solid $Br=0.1$. (a) velocity, (b) temperature. (Top to bottom).

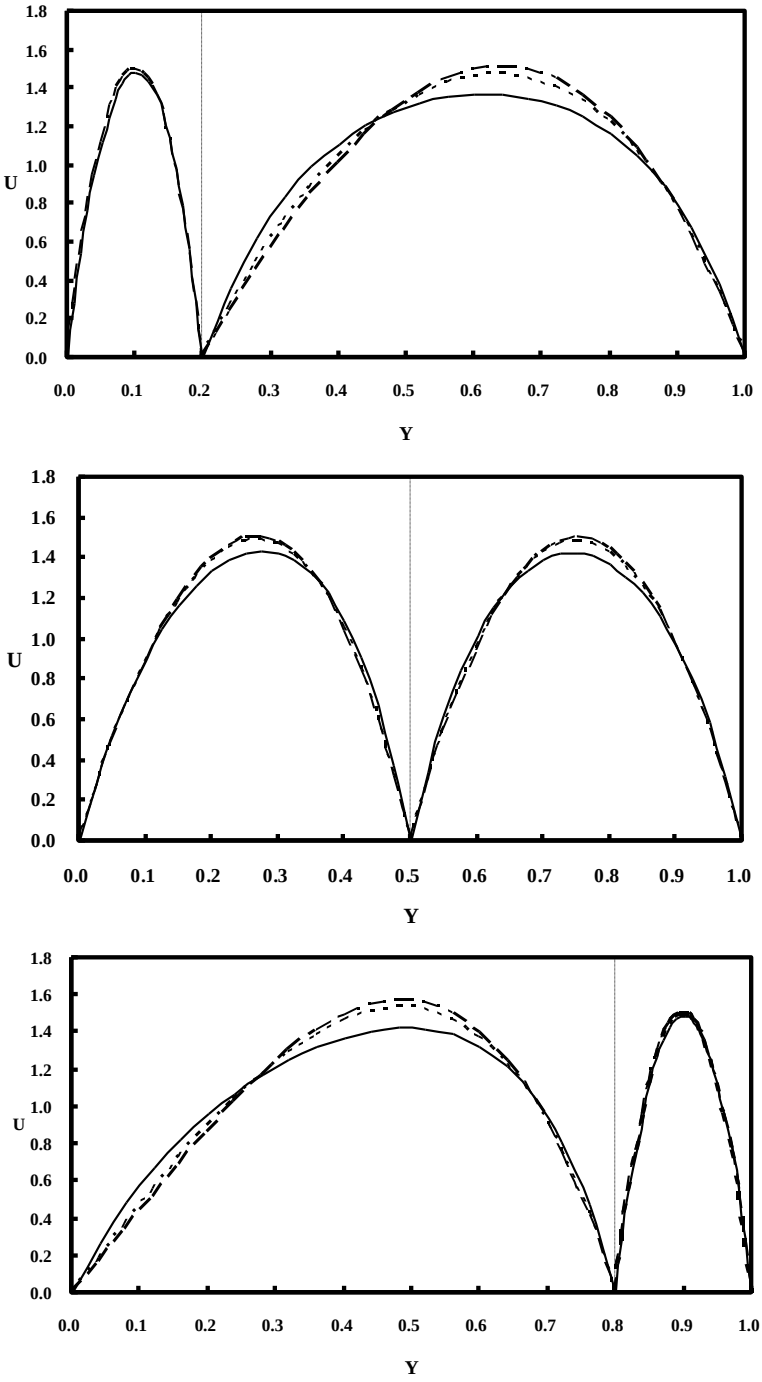

Figure 3. Velocity profiles for various values of Y^* with $Gr/\mathrm{Re}=50$, $Br=0.05$, $m=1$; dashed $\sigma=2$, dotted $\sigma=4$, solid $\sigma=8$. (a) $Y^*=0.2$, (b) $Y^*=0.5$, (c) $Y^*=0.8$. (Top to bottom).

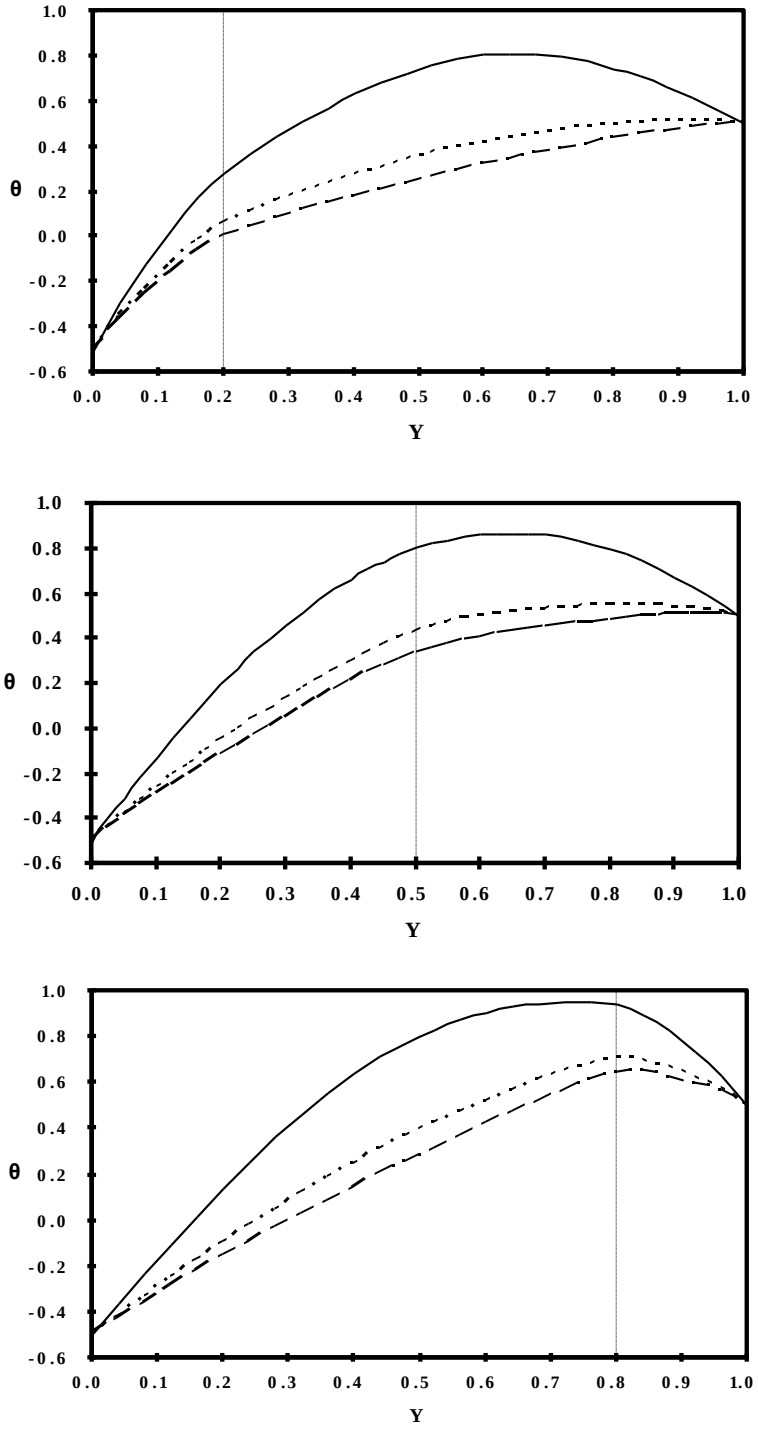

Figure 4. Temperature profiles for various values of Y^* with $Gr/\mathrm{Re}=50$, $Br=0.05$, $m=1$; dashed $\sigma=2$, dotted $\sigma=4$, solid $\sigma=8$. (a) $Y^*=0.2$, (b) $Y^*=0.5$, (c) $Y^*=0.8$. (Top to bottom).

Since the effect of Brinkman number on the velocity and temperature profiles has been investigated in Salah El-Din [13], a brief description is delivered here. Increasing the value of Br results in an enhancement of the temperature profiles for three baffle positions (Y^* = 0.2, 0.5 and 0.8) and the derivation from a linear profile, owing to strong dissipative effects is observed. The difference or distortion in the velocity distributions for different values of Br can be observed in the wider passage and in equal passages, and not be discernible in the narrower passage for the balancing effect of increasing the buoyancy force and decreasing the driving pressure gradient.

Figures 3 and 4 show the velocity and temperature profiles, respectively, for porous parameters σ = 2, 4 and 8 at three different baffle positions (Y^* = 0.2, 0.5 and 0.8) with $Gr/\mathrm{Re} = 50$, $Br = 0.05$ and $m = 1$. Since the so-called Darcy-Brinkman equation is assumed to be valid in the present study, the case of vanishing porous parameter $\sigma \to 0$ can be used to compare with the clear fluid while the case of infinity σ reduces to Darcy's equation. Thus, the porous parameter may be treated as measure of the drag force for fluid flow in a porous medium. As expected, the maximum of the velocity profile decreases for increasing values of σ in the wider passage for both $Y^* = 0.2$ and $Y^* = 0.8$, showing the dragging effect of the Darcy resistance on porous-fluid channel flow. In addition, the velocity profiles near both walls increase correspondingly due to the conservation of mass which reflects the constraint of Eqs. (10) and (11). The difference between the velocity profiles for varying σ can not be discernible in the narrower passage, as noted previously. For $Y^* = 0.5$, the distortion effect of σ on velocity profile is also observable. With increasing values of σ, the temperature profiles augment in both passages for the increasing amount of heat generated by Darcy and viscous dissipations.

The effect of the buoyancy-to-inertial force (mixed convection parameter) Gr/Re on the velocity and temperature fields for various baffle positions is displayed in Figs. 5 and 6, respectively, with $\sigma = 2$, $Br = 0.01$ and $m = 1$. For each graph the maximum point of the velocity profile moves to the right (hotter) wall for increasing values of Gr/Re and thus, the velocity decreases near the left (colder) wall. The larger the value of Gr/Re, the stronger the upward velocity. Especially, for sufficient large values of Gr/Re, the flow reversal is found near the left wall shown in Fig. 5(c), which can also be observed even in the single passage flow examined by Aung and Worku [22]. Since the Brinkman number taken in these figures is small, the temperature profile is nearly linear. It is seen that the temperature profiles are slightly enhanced for increasing Gr/Re in the wider passage and are less discernable in the narrower passage.

The effect of the viscosity ratio m on the velocity and temperature distributions is shown in Figures 7 and 8, for three baffle positions with $Gr/\mathrm{Re} = 50$, $\sigma = 2$ and $Br = 0.05$. Physically, $m > 1$ denotes that the viscosity of the Darcy's term is larger than the effective viscosity of the Brinkman term in the momentum equation. It can be observed that the maximum point of the velocity profile shifts to the right wall for larger m since the effective viscosity is lowered in this case, and the temperature profile decreases with increasing values of m. From Eq. (8), it is expected that the increase in the Brinkman number and the porous parameter leads to an increase in the temperature profile, however, an increase in the viscosity ratio reduces it. This explains the results in Figures 4 and 8.

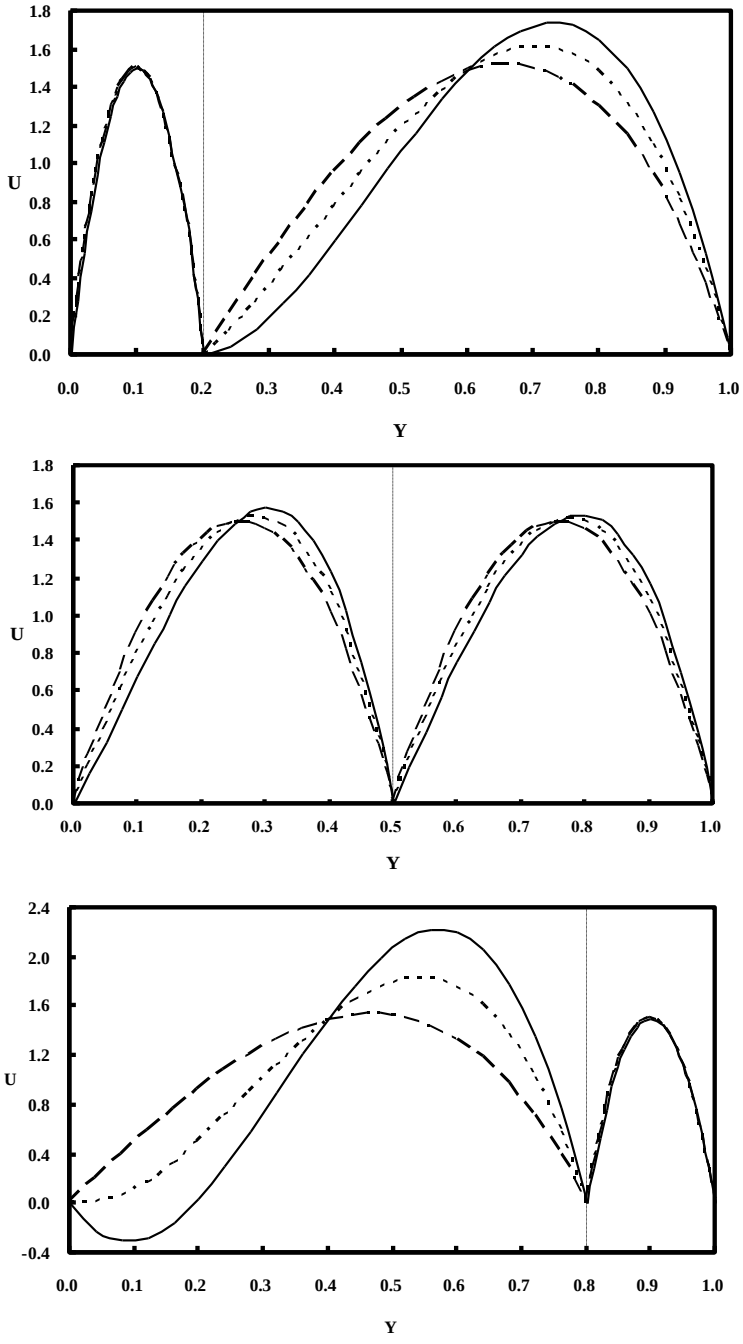

Figure 5. Velocity profiles for various values of Y^* with $\sigma = 2$, $Br = 0.01$, $m = 1$; dashed $Gr/\mathrm{Re} = 50$, dotted $Gr/\mathrm{Re} = 150$, solid $Gr/\mathrm{Re} = 250$; (a) $Y^* = 0.2$, (b) $Y^* = 0.5$, (c) $Y^* = 0.8$. (Top to bottom).

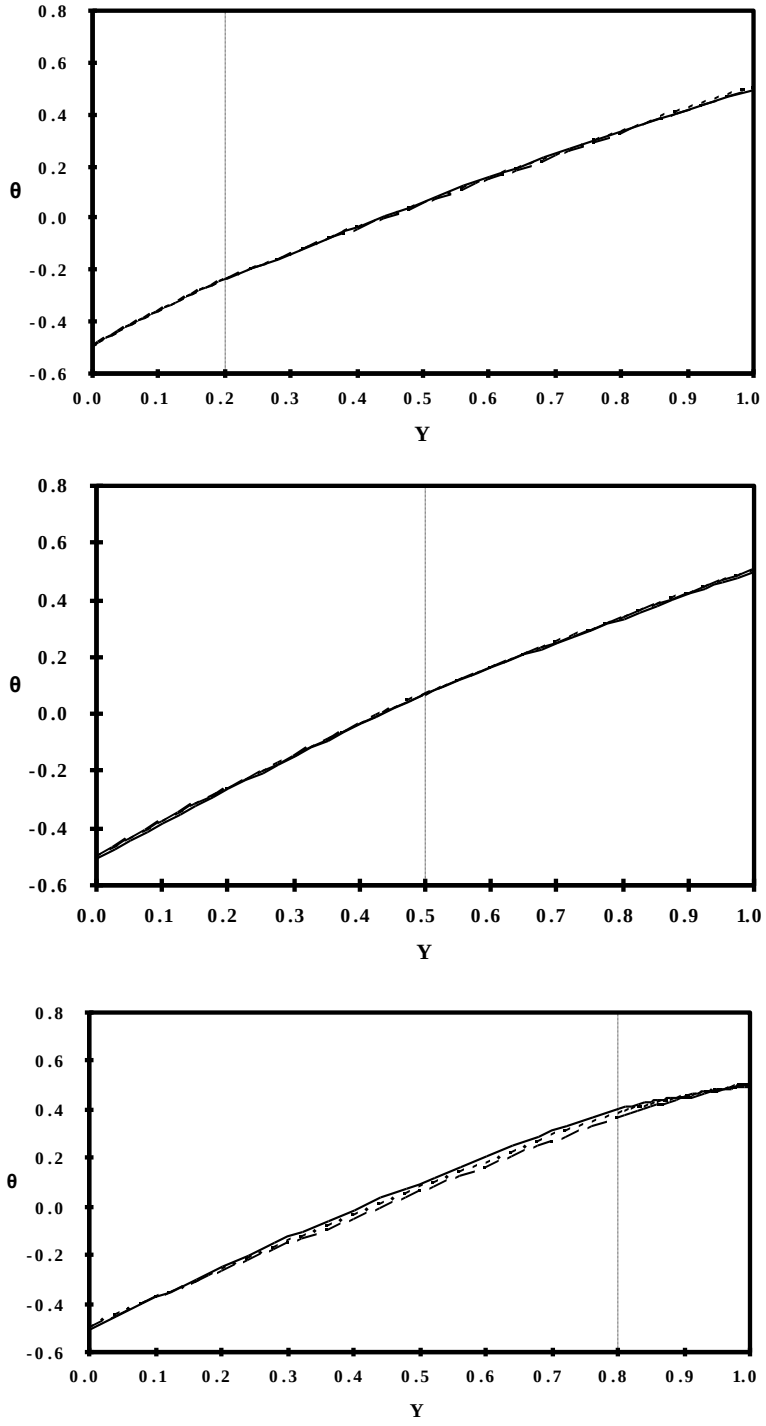

Figure 6. Temperature profiles for various values of Y^* with $\sigma = 2$, $Br = 0.01$, $m = 1$; dashed $Gr/\mathrm{Re} = 50$, dotted $Gr/\mathrm{Re} = 150$, solid $Gr/\mathrm{Re} = 250$; (a) $Y^* = 0.2$, (b) $Y^* = 0.5$, (c) $Y^* = 0.8$. (Top to bottom).

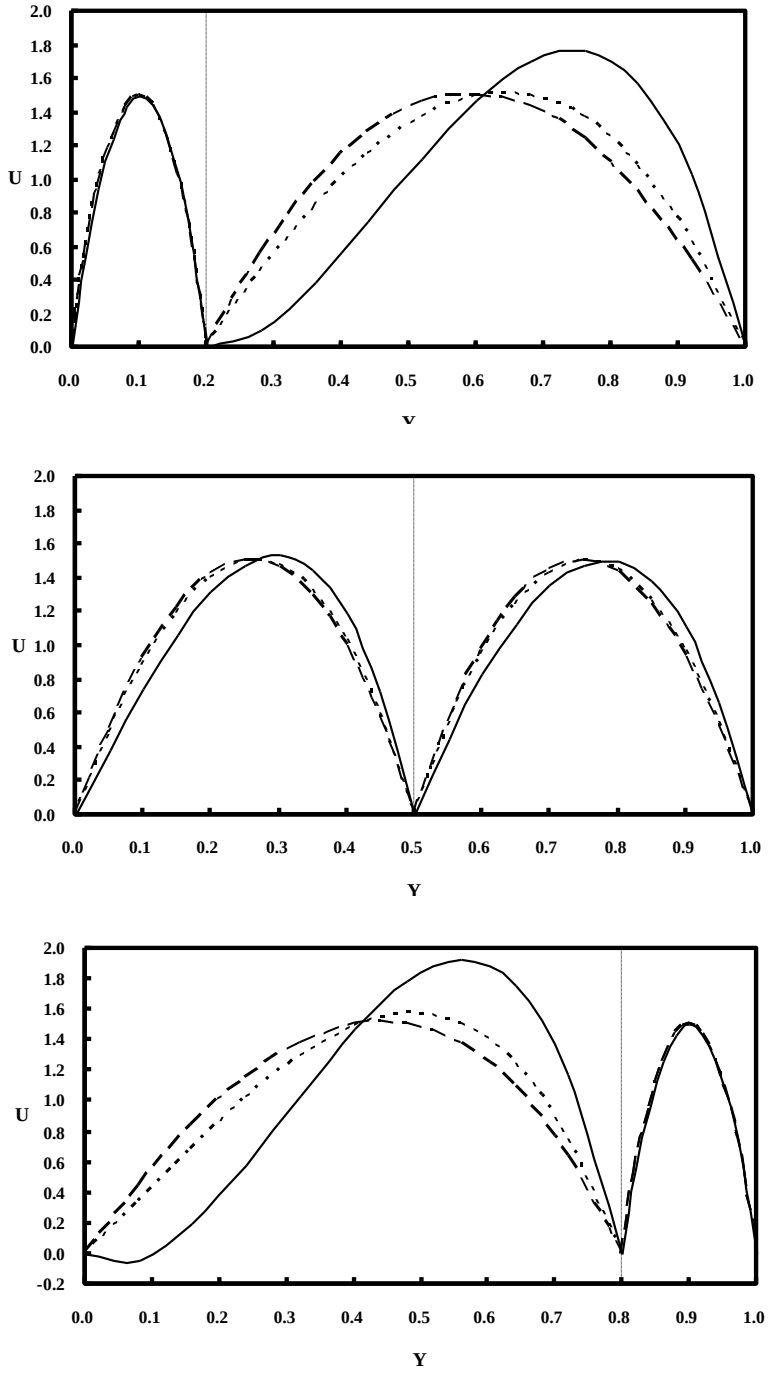

Figure 7. Velocity profiles for various values of m with $Y^* = 0.5$, $Gr/\mathrm{Re} = 50$, $\sigma = 2$, $Br = 0.05$; dashed $m = 0.5$, dotted $m = 1$, solid $m = 2$ (a) $Y^* = 0.2$, (b) $Y^* = 0.5$, (c) $Y^* = 0.8$. (Top to bottom).

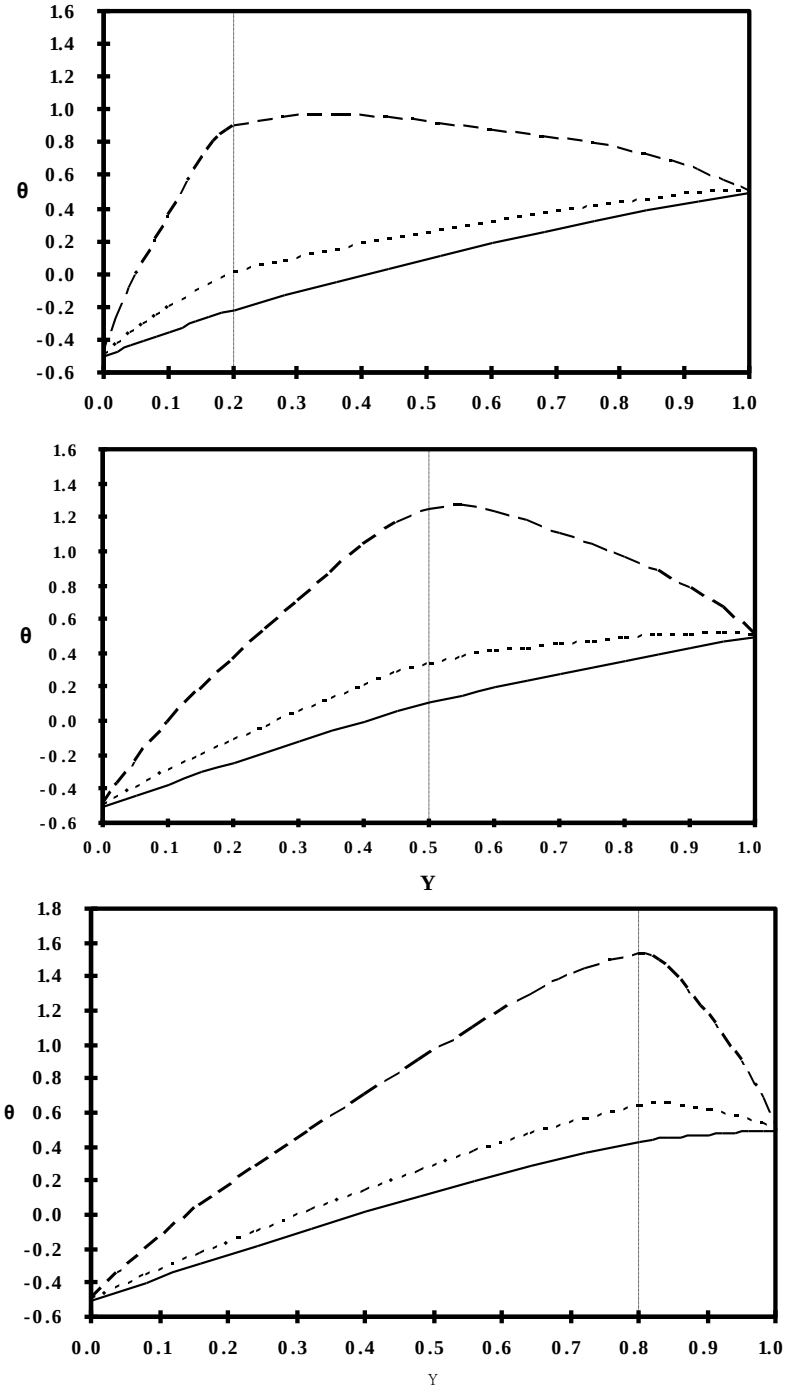

Figure 8. Temperature profiles for various values of m with $Y^* = 0.5$, $Gr/\mathrm{Re} = 50$, $\sigma = 2$, $Br = 0.05$; dashed $m = 0.5$, dotted $m = 1$, solid $m = 2$ (a) $Y^* = 0.2$, (b) $Y^* = 0.5$, (c) $Y^* = 0.8$. (Top to bottom).

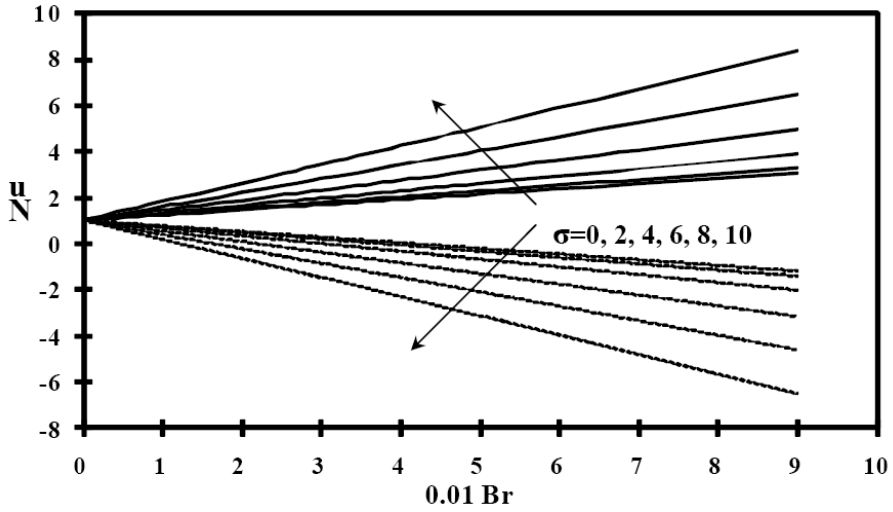

Figure 9. Nusselt numbers for various values of σ and Br with Y^* =0.5, Gr/Re =50 and m =1; solid- Nu_c , dashed- Nu_h .

In Figure 9, the Nusselt numbers at the cold (Nu_c) and the hot walls (Nu_h) versus the Brinkman number with $Y^* = 0.5$, $Gr/\mathrm{Re} = 50$ and $m = 1$ for selected porous parameter values are illustrated. It is apparent that an increase in the values of the porous parameter σ leads to enlargements for both the magnitudes of Nu_c and Nu_h , and the variations of heat flux to Br for each value of σ are nearly linear. This behavior is similar to a linear variation of Nu versus Br for a pure viscous fluid, meaning that the temperature profiles are distorted for a fluid-saturated porous medium in a similar way like that for a pure viscous fluid (Salah El-Din [13]).

In a following paper, the constraint of flow rates within the two-passage channel used by Cheng et al. [6] will be employed for a much broader range of validity rather than those employed in the present study, i.e. Eqs. (10) and (11).

CONCLUSION

The characteristics of flow and heat transfer of fluid-saturated porous medium in a double-passage channel with a perfectly conductive baffle are investigated. According to the results, the following conclusions can be drawn:

1. The maxima of velocity profiles are lessened for increasing values of the porous parameter, and the velocity profiles are distorted by the effects of the porous parameter, Gr/Re , viscosity ratio and the Brinkman number, especially in the wider passage.
2. The temperature profiles increase as both the porous parameter and the Brinkman number increase but decrease as the viscosity ratio increases. Again, these effects are more pronounced in the wider passage than in the narrower passage of the channel.

3. The variations of the Nusselt number at both the cold and the hot walls to Brinkman number are also nearly linear even in the presence of the fluid-saturated porous medium. The heat transfer rates at both walls are enhanced for increasing values of the porous parameter since the dissipation effect becomes stronger.

REFERENCES

[1] A. E. Bergles, Applications of Heat Transfer Augmentation, In: S. Kakac, A.E. Bergles, F. Mayinger, Editors, *Heat Exchangers: Thermal–Hydraulic Fundamentals and Design*, Hemisphere, New York, pp. 883-911, 1981.

[2] J. P. Gupta, *Fundamentals of Heat Exchanger and Pressure Vessel Technology*, Hemisphere, New York, pp. 22-33, 1986.

[3] R. L. Webb, *Principles of Enhanced Heat Transfer*, Hemisphere, New York, pp. 3-11 1994.

[4] Z. Y. Guo, D.Y. Li, B.X. Wang, A novel concept for convective heat transfer enhancement, Int. J. Heat Mass Transfer 41 (1998) 2221-2225.

[5] C. P. Tso, S.P. Mahulikar, The use of Brinkman number for single phase forced convective heat transfer in microchannels, *Int. J. Heat Mass Transfer* 41 (1998) 1759-1769.

[6] C. H. Cheng, H.S. Kuo, W.H. Huang, Laminar fully developed forced-convection flow within an asymmetric heated horizontal double-passage channel, *Appl. Energy* 33 (1989) 265-286.

[7] M. M. Salah El-Din, Fully developed laminar convection in a vertical double-passage channel, *Appl. Energy* 47 (1994) 69-75.

[8] Z. Y. Guo, D.Y. Li, B.X. Wang, A novel concept for convective heat transfer enhancement, *Int. J. Heat Mass Transfer* 41 (1998) 2221-2225.

[9] Z. D. Chen, J.J.J. Chen, Local heat transfer for oscillatory flow in the presence of a single baffle within a channel, *Chem. Eng. Sci.* 53 (1998) 3177-3180.

[10] K. Shiina, S. Nakamura, S. Matsumura, Enhancement of shell side forced convective heat transfer in the shell tube-type heat exchanger using thin plate-type supports, *Heat Transfer-Asian Research* 32 (2003) 455-471.

[11] T. S. Chang, Y.H. Shiau, Flow pulsation and baffle's effects on the opposing mixed convection in a vertical channel, *Int. J. Heat Mass Transfer* 48 (2005) 4190-4204.

[12] P. Dutta, A. Hossain, Internal cooling augmentation in rectangular channel using two inclined baffles, *Int. J. Heat Fluid Flow* 26 (2005) 223-232.

[13] M. M. Salah El-Din, Effect of viscous dissipation on fully developed laminar mixed convection in a vertical double-passage channel, *Int. J. Therm. Sci*. 41 (2002) 253-259.

[14] C. L. Tien, K. Vafai, Convective and radiative heat transfer in porous media, *Adv. Appl. Mech.* 27 (1989) 225-281.

[15] A. Amiri, K. Vafai, Effects of boundary conditions on non-Darcian heat transfer through porous media and experimental comparisons, *Num. Heat Transfer* 27 (1995) 651-664.

[16] P. D. Weidman, A. Medina, Porous media convection between vertical walls: continuum of solutions from capped to open ends, *Acta Mech*. 199 (2008) 209-216.

[17] D. A. Nield, A. Bejan, *Convection in Porous Media*, 3rd ed., Springer, New York, 2006.
[18] K. R. Rajagopal, M. Ruzicka, A.R. Srinivasa, On the Oberbeck-Boussinesq approximation, *Math. Meth. Appl. Mech*. 6 (1996) 1157-1167.
[19] A. Barletta, Laminar mixed convection with viscous dissipation in a vertical channel, *Int. J. Heat Mass Transfer* 41 (1998) 3501-3513.
[20] R. C. Gilver, S.A. Altobelli, A determination of effective viscosity for the Brinkman-Forchheimer flow model, *J. Fluid. Mech*. 258 (1994) 355–370.
[21] A. Barletta, E. Zanchini, On the choice of the reference temperature for fully-developed mixed convection in a vertical channel, *Int. J. Heat Mass Transfer* 42 (1999) 3169-3181.
[22] W. Aung, G. Worku, Theory of fully developed, combined convection including flow reversal, *J. Heat Transfer* 108 (1986) 485-488.

Received 19 November 2012; received in revised form 09 December 2013; accepted 12 December 2013.